ACS APPLIED MATERIALS & INTERFACES

www.acsami.org

Research Article

Hybrid Janus Membrane with Dual-Asymmetry Integration of Wettability and Conductivity for Ultra-Low-Volume Sweat Sensing

Xiao Hong, Huimin Wu, Chengcheng Wang, Xinran Zhang, Chenjie Wei, Zhikang Xu, Dajing Chen,* and Xiaojun Huang*

Cite This: *ACS Appl. Mater. Interfaces* 2022, 14, 9644−9654

Read Online

ACCESS | Metrics & More | Article Recommendations | Supporting Information

ABSTRACT: Highly sensitive and selective analysis of sweat at ultra-low sample volume remains a major challenge in the field of biosensing. Manipulation of small volumes of liquid for efficient sampling is essential to address this challenge. A hybrid Janus membrane with dual-asymmetry integration of wettability and conductivity is developed for regulated micro-volume liquid transport in wearable sweat biosensing. Unlike the uncontrollable liquid diffusion in a conventional porous membrane, the asymmetric wettability of porous Janus membrane leads to unique unidirectional liquid transport with high breakthrough pressure (1737.66 Pa) and fast self-pumping rate (35.94 μL/min) for micro-volume liquid sampling. The asymmetric conductive layer shows excellent flexible conductivity, anti-interference of friction, and efficient electrochemical interface due to the in situ generation of gold nanoparticles on one side of the membrane. The fabricated Pt-enzyme electrodes on the membrane promises effective testing range, great selectivity, and high sensitivity and accuracy (correlation efficiency, glucose: R^2 = 0.999, lactate: R^2 = 0.997), enabling ultra-low volume (~0.15 μL) real time measurements on the skin surface. The innovative Janus membrane with unidirectional, self-pumping, and anti-interference performance provides a new strategy for miniaturized wearable microfluidic sweat electrochemical biosensor preparation in athletic performance evaluation, health monitoring, disease diagnosis, intelligent medicine, and so forth.

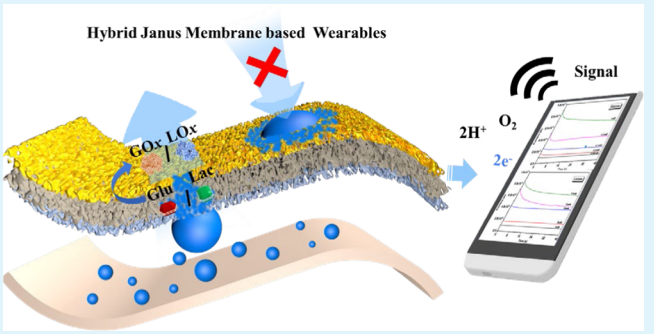

KEYWORDS: *Janus membrane, bi-anisotropic conductivity, unidirectional liquid transport, ultra-low volume, wearable electrochemical biosensor*

1. INTRODUCTION

With increasing concerns about individual healthcare and personal security, wearable biosensors have attracted significant attention as new analytical tools for condition monitoring, due to the advantages of miniaturization, portability, non-invasiveness, and instantaneity.[1−5] To date, apart from the physical parameters and environmental risks, physiological information also has been monitored to meet the growing needs in personalized medicine, precise diagnosis, and athletic monitoring.[6−11] Sweat, one of the easily accessible biofluids providing rich physiological information, is primarily composed of water, electrolytes (sodium, calcium, potassium, magnesium, zinc, and chlorides), nitrogenous compounds (urea and amino acids), proteins, and metabolites (creatinine, uric acid, glucose, and lactate).[12−14] Sweat analysis faces various technical challenges, including low sample volume, complex composition of test objects, and non-static testing conditions.[15−19]

In recent years, great advances in wearable sweat biosensors based on different detection approaches have been achieved for in situ monitoring of chemical and biological biomarkers in sweat.[20−23] Significant progress has taken place in the way of sample capture. To address the problem of unavoidable physical frictional interference caused by direct contact between human epidermis and conductive sensing element, researchers have proposed different sampling strategies using well-designed microchannels or porous absorbent materials to achieve indirect contact of sensing layers with skin.[24−26] Compared with the costly and complicated fabrication of microchannels in traditional microfluidic devices, porous materials (e.g., textiles and papers) have been proposed to simplify the microfluidic channel fabrication process in wearable sweat biosensors.[27−30] Among them, porous textiles can be used for efficient sample collection and flexible electrode preparation in wearable sweat biosensors.[13,31−34] Nevertheless, due to the homogeneous hydrophilic structure with a disordered micro-liquid channel in three-dimensional

Received: September 1, 2021
Accepted: January 21, 2022
Published: February 8, 2022

https://doi.org/10.1021/acsami.1c16820
ACS Appl. Mater. Interfaces 2022, 14, 9644−9654

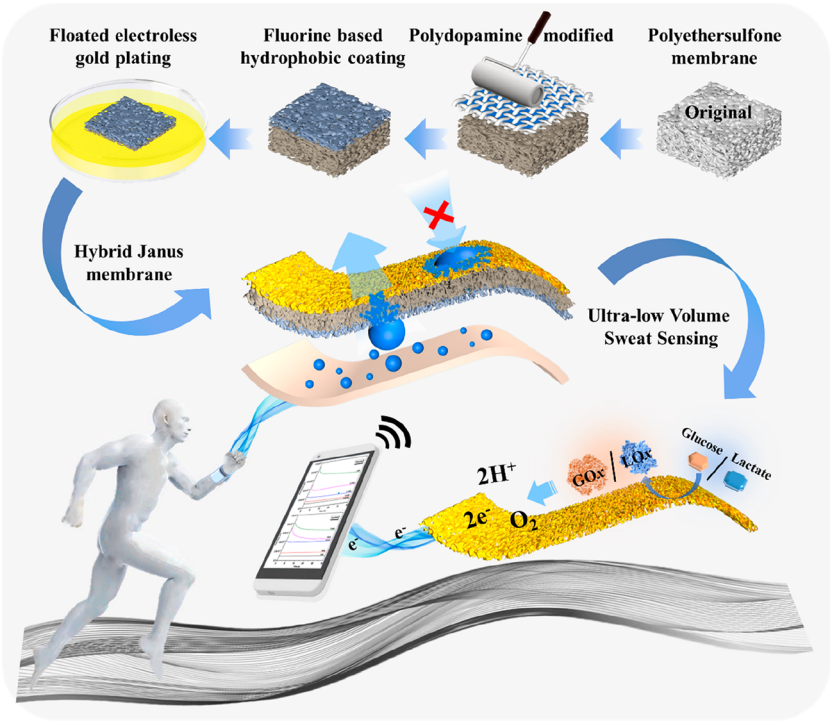

Figure 1. Schematic diagram of the HJM with dual-asymmetry integration of wettability and conductivity for wearable electrochemical sweat monitoring.

porous textiles, uncontrollable liquid surface diffusion causes sample loss and large sampling volume to perform analysis (at least 10−100 μL) as well as undesirable contamination problems caused by the backflow of water-soluble chemical agents.[35−37] To address the problem of sample loss, introducing an asymmetric hydrophobic/hydrophilic interface combined with well-designed microchannels has been proposed by traditional microfluidic devices to realize the micro-liter or nano-liter volume sweat detection.[23,38] Besides, appropriate microchannels in the three-dimensional porous materials also influence the dynamic liquid transportation. The development of various materials (e.g., membrane with micro-pore size) is a useful way to achieve an ideal low-volume wearable sweat analysis. Our previous work realized the successful introduction of asymmetry wettability in the thickness direction into microfiltration membrane. Combined with Janus interface and micro-pore size, controllable micro-volume liquid transport function has been brought about in glucose detection, but is not directly applicable to wearable sweat biosensors.[39] Currently, it is still a challenge for wearable microfluidic biosensors to detect low-concentration biomarkers at ultra-low sample volumes (<1 μL) in real time.

Herein, inspired by Janus microfluidic interface of cell membranes with liquid transmission capability, a hybrid configuration with asymmetry wettability and bi-anisotropic conductivity for ultra-low-volume, high precision, membrane-based wearable sweat electrochemical biosensor was developed (as shown in Figure 1). The asymmetric wettability of the hybrid Janus membrane (HJM) was prepared by successive dip-coating [polydopamine (PDA)] and roller-assisted liquid printing (fluoropolymer), achieving unidirectional liquid transport and self-pumping micro-volume sample collection without backflow contaminations. The asymmetric conductive layer composed of in situ-generated gold nanoparticles was developed by interfacial floating combined with platinum colloid catalyzed electroless plating, resulting in excellent flexible conductivity and anti-interference based on nondirect contact mass transfer. In summary, membrane-based Pt-enzyme-HJM electrodes were developed for electrochemical testing of glucose and lactate, two common metabolites in sweat. This study has developed a new strategy in lightweight wearable electrochemical biosensors for ultra-low-volume sweat analysis, which can be further applied to athletic performance evaluation, health monitoring, disease diagnosis, intelligent medicine, and so forth.

2. EXPERIMENTAL SECTION

2.1. Materials. Polyethersulfone (PES) flat sheet membranes (average pore size 0.95 μm) were supplied by O'Happure Membrane Technology Co., Ltd. (Nanjing, China). Dopamine hydrochloride (DA, 98%), potassium ferricyanide {$K_3[Fe(CN)_6]$, AR}, potassium ferrocyanide trihydrate {$K_4[Fe(CN)_6]\cdot 3H_2O$, AR), coumarin 6 (HPLC), and rhodamine B (AR) were produced from Aldrich (Shanghai, China). Petroleum ether (60−90 °C, AR), ethanol (AR), hydrochloric acid (HCl, AR), potassium chloride (KCl, AR), disodium hydrogen phosphate (Na_2HPO_4, AR), potassium dihydrogen phosphate (KH_2PO_4, AR), sodium borohydride ($NaBH_4$, AR), cupric sulfate ($CuSO_4$, AR), urea (AR), lactate (AR), glucose (AR), ascorbic acid (AR), pyronin G (BR), hydrogen peroxide 30% aqueous solution (H_2O_2, AR), 25% glutaraldehyde solution (GA, BR), and polyvinylpyrrolidone K30 (PVP K 30, GR) were all obtained from Sinopharm Chemical Reagent Co., Ltd. (China). Chloroplatinic acid hexahydrate ($H_2PtCl_6\cdot 6H_2O$, AR), lead (II) acetate trihydrate [$Pb(CH_3COO)_2\cdot 3H_2O$, AR], chloroauric acid ($HAuCl_4$), and stearyl trimethyl ammonium chloride (STAC, AR) were all purchased from Macklin Biochemical Co., Ltd. (Shanghai, China). Glucose oxidase (GOx, 239 U/mg) from *Aspergillus niger* was supplied by Yuanye Biotech Co., Ltd. (Shanghai, China). Lactate oxidase (LOx, ≥90 U/mg) from *Aerococcus viridans* was produced from Sangon Biotech Co., Ltd. (Shanghai, China). The commercial hydrophobic fluorine-based waterproof spray TS-10 was purchased from Guangdong Hec Technology Holding Co., Ltd (Guangdong,

https://doi.org/10.1021/acsami.1c16820
ACS Appl. Mater. Interfaces 2022, 14, 9644−9654

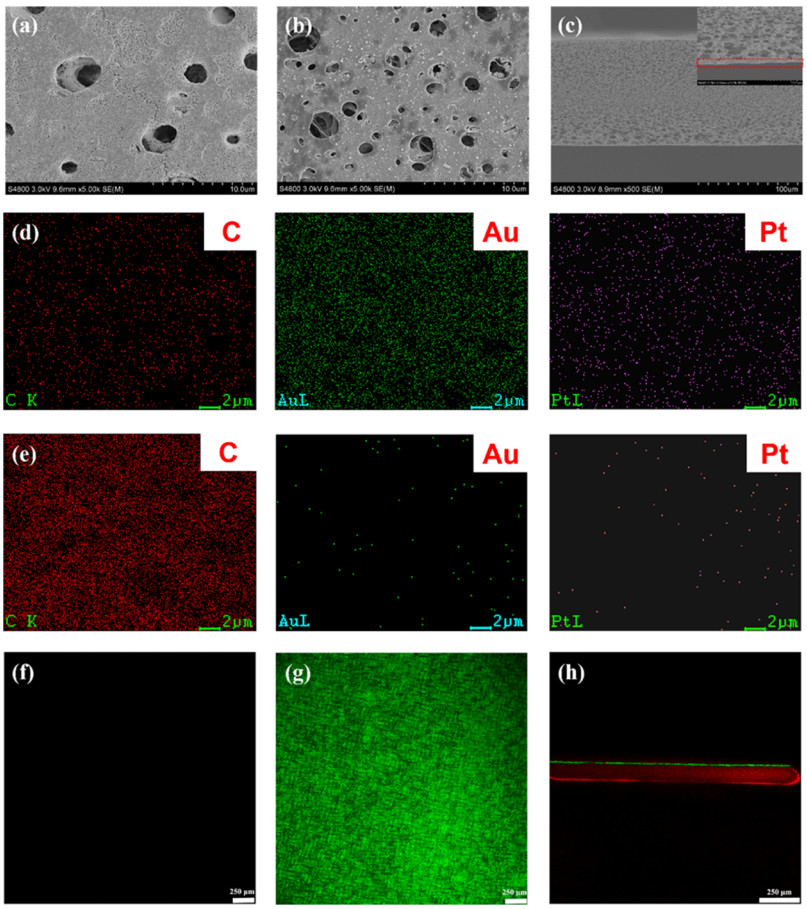

Figure 2. Dual-asymmetry integration structure. (a−c,f−h) Surface and cross-sectional morphologies of HJM by SEM and LCSM. Carbon (C), gold (Au), and platinum (Pt) elements distribution on the surface of HJM by EDX. (a,d,f) Conductive (hydrophilic) surface; (b,e,g) Insulate (hydrophobic) surface. For LCSM observation, the hydrophobic layer was dyed with coumarin 6. The hydrophilic side was dyed with rhodamine B for better observation of asymmetric wettability gradient in the cross section of HJM.

China). Tris(hydroxymethyl)aminomethane (Tris, UP) was obtained from Amresco (OH, USA). The commercial nylon mesh (average pore size 25 μm) was purchased from market and used as a porous substrate to transfer hydrophobic coating by liquid surface tension. All of these reagents were used without further purification.

2.2. Membrane Preparation. The HJM with asymmetric wettability and conductivity was prepared by asymmetric modification. First, basic Janus membrane (BJM) with asymmetric wettability was prepared by successive dip-coating (PDA) and roller-assisted liquid printing (hydrophobic coating). PES membrane was immersed into Tris-HCl solution containing 2 mg/mL dopamine at 25 °C to form a PDA layer. After 24 h deposition, the PDA-coated membrane was thoroughly washed by deionized water for 8 h, followed by the asymmetric hydrophobic modification of TS-10 fluoropolymer by roller-assisted liquid printing three times. A commercial nylon mesh was used as the medium of hydrophobic liquid transfer. Second, HJM was fabricated from BJM by electroless gold plating catalyzed by platinum colloid. Due to the enhanced interface floated performance of BJM (Figure S1), the asymmetric conductivity of HJM could be derived from floating and reacting on the surface of electroless gold plating bath. For the preparation of Pt colloids sol, 0.05 mM $H_2PtCl_6 \cdot 6H_2O$ and 10 mg PVP were dissolved in 96.5 mL water. Then, 1 mL of 0.2 mM $NaBH_4$ was poured into the mixture with vigorous stirring, and the solution was left to stand at room temperature for 24 h before use. BJM was floated on 1 mg/mL STAC solution for 1 min and Pt colloid sol for 10 min to immobilize Pt nanoparticles on the membrane surface, respectively. After drying for several minutes at room temperature, the membrane was floated on a plating bath containing 10 mM $HAuCl_4$ and 20 mM H_2O_2 for 1 h. The reaction of Pt nanoparticles facilitates gold deposition, as shown in eq 1[40]

$$2HAuCl_4 + 3H_2O_2 \xrightarrow{Pt} 2Au + 2O_2 + 8HCl \quad (1)$$

Thus, a nanostructure conductive BJM with asymmetric wettability and conductivity was successfully prepared.

2.3. Membrane Characterization. Field emission scanning electron microscopy (SEM; Hitachi S4800, Shimadzu) with an energy-dispersive X-ray detector was conducted to observe the surface morphologies and element distributions of membranes. Attenuated total reflectance Fourier transform infrared spectroscopy (ATR−FTIR; Nicolet 6700, Thermo Fisher) and X-ray photoelectron spectroscopy (XPS; PHI-5000C, PerkinElmer) were performed to analyze the chemical structures and compositions of membranes. Laser confocal scanning microscopy (LCSM; TCS SP5, Leica) was used to distinguish the asymmetric structure of the Janus membrane by dying with certain fluorochromes (coumarin 6 and rhodamine B). The water contact angles (WCA) of membranes were measured by a contact angle system (DropMeter A-100P, MAIST Vision Inspection & Measurement Co., Ltd). The volume of the water droplet was set at 5 μL. An electrochemical workstation (CHI660a, CH Instruments) was used to take all the electrochemical measurements at room temperature. Ag/AgCl and Pt wire were used as reference electrode and counter electrode, respectively.

2.4. Determination of Water Flux. A lab-made scale device was used to evaluate the flow rate of water through membrane at different pressures. The minimum hydrostatic pressure (breakthrough pressure, $P_{B.P}$) was evaluated based on the water flux. The water flux (F) was calculated using eq 2.

$$F = \frac{V}{A*t*P} \quad (2)$$

https://doi.org/10.1021/acsami.1c16820
ACS Appl. Mater. Interfaces 2022, 14, 9644−9654

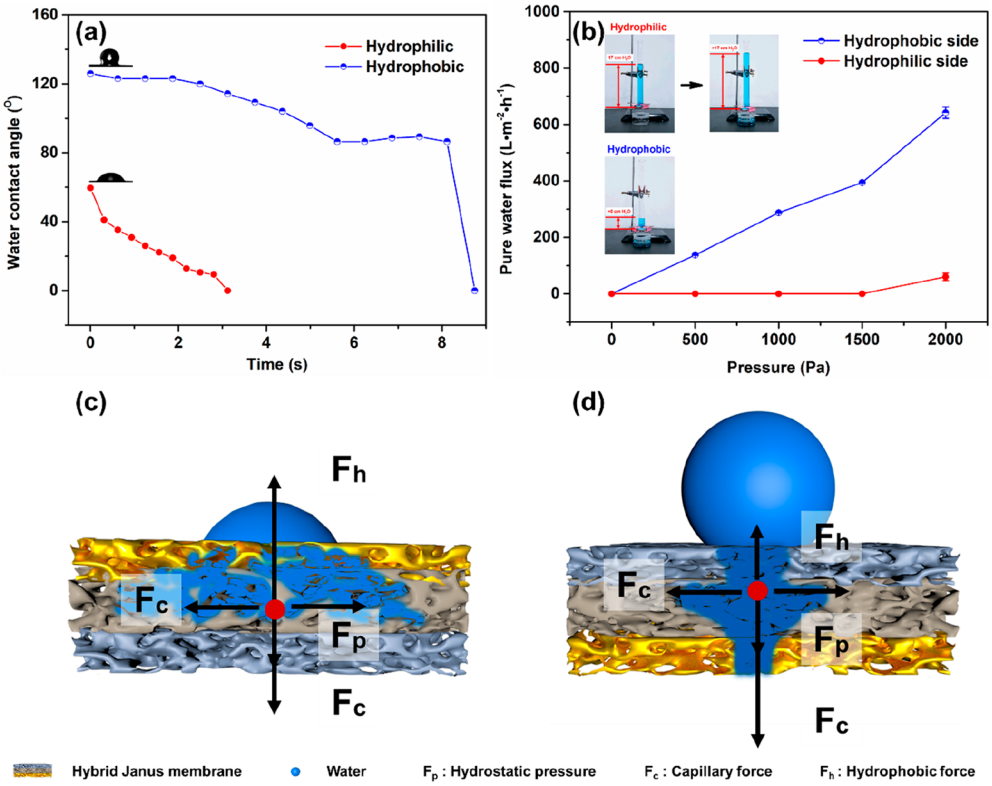

Figure 3. Asymmetric wettability and unidirectional liquid transport performance. (a) Evolution of WCAs; (b) pure water flux for both sides of HJM; (c,d) diagram of force analysis when water permeated from hydrophilic side and hydrophobic side. The main imbalanced forces involved in unidirectional liquid transport process are the hydrostatic pressure (F_P), hydrophobic force (F_h) and capillary force (F_c).

where V, A, t, and P are the volume of permeate liquid, the effective membrane filtration area, time, and applied pressure, respectively.

2.5. Fabrication of Nanostructure Pt-Enzyme-HJM Electrode. At first, the conductive HJM was immersed in a solution containing 0.5 M HCl, 2.5 mg/mL H_2PtCl_6, and 1.85 mg/mL $Pb(CH_3COO)_2$ for the electrodeposition of Pt nanoparticles onto the Au nanostructure at 2.5 V for 300 s. The electrodeposited Pt nanoparticles were used for catalytic reaction and improved the sensitivity of the electrode.

Second, enzyme-immobilized HJM membrane after Pt nanoparticle electrodeposition was needed for glucose and lactate detection. The enzyme immobilization process on the HJM membrane is mainly based on physical adsorption combined with chemical cross-linking. Glutaraldehyde was selected as a chemical cross-linking agent for further cross-linking the adsorbed enzyme aggregates to achieve an excellent and durable product. The optimization of enzyme content was decided after experiments (Figure S2). For glucose detection, a mixture solution of GOx (1 wt %) and GA (1 wt %) was pre-cross-linked before 5 μL solution was coated on the surface of the electrode after Pt nanoparticle electrodeposition and repeated twice. When detecting lactate, LOx (0.5 wt %) was directly coated on the surface of the electrode twice and then further cross-linked by GA (1 wt %). All the modified Pt-enzyme-HJM electrodes were dried at 37 °C for 0.5 h after enzyme immobilization process and stored at 4 °C when not in use.

2.6. Pt-Enzyme-HJM Electrode Performance Test. All the in vitro tests of glucose and lactate were carried out in a PBS solution (pH 7.4). The corresponding $I-t$ response curves were recorded in 40 mL PBS under 0.5 V working potential with different concentrations of glucose or lactate added every 300 s. The electroactivity of the electrode was evaluated by recording cyclic voltammogram (CV) in a 0.1 M NaCl solution containing 5 mM $Fe(CN)_6^{3-/4-}$ in the potential range from −0.2 to +0.5 V.[41] The artificial sweat was formed with 10 mM Na_2HPO_4, 1.75 mM KH_2PO_4, 137 mM NaCl, 2.65 mM KCl, and different concentrations of glucose/lactate.[8,20] The simulated perspiration and metabolite detection test were taken on the surface of a planar filter paper by adding different concentrations of glucose/lactate. The in situ tests of glucose and lactate were performed on the skin, while a certain volume of artificial sweat was used to pre-wet the epidermis. The experiments were approved by the Institutional Research Ethics Committee of Hangzhou Normal University (2020-7001). The glucose/lactate was then oxidized by GOx or LOx, and the resultant electrooxidation current (eqs 3−5) was recorded with CHI260 electrochemical workstation.[42,43]

$$\text{Glucose} + O_2 + H_2O \xrightarrow{\text{GOx}} \text{gluconic acid} + H_2O_2 \quad (3)$$

$$\text{Lactate} + O_2 \xrightarrow{\text{LOx}} \text{pyruvic acid} + H_2O_2 \quad (4)$$

$$H_2O_2 \xrightarrow{\text{Pt}} 2H^+ + O_2 + 2e^- \quad (5)$$

3. RESULTS AND DISCUSSION

3.1. Structure of the HJM Membranes. The microstructure and material composition have significant influence on both liquid transportation and electrochemistry performances. Compared with the original membrane and BJM in Figure S3, the conductive/hydrophilic surface of HJM (Figure 2a) was covered with a layer of particles with the diameter range of 80−165 nm without blocking the original membrane pore. Only few local aggregations of particles were observed on the insulate/hydrophobic surface of HJM (Figure 2b). From the cross-sectional image of HJM (Figure 2c), the thickness of the continuous nanoparticles layer was about 35 nm. Besides, a highly porous and sponge-like structure was also observed in the cross-sectional image, which was important for the efficient sweat up-taking and sensitive electrochemical detection. The composition of the continuous nanoparticle layer could be

https://doi.org/10.1021/acsami.1c16820
ACS Appl. Mater. Interfaces 2022, 14, 9644−9654

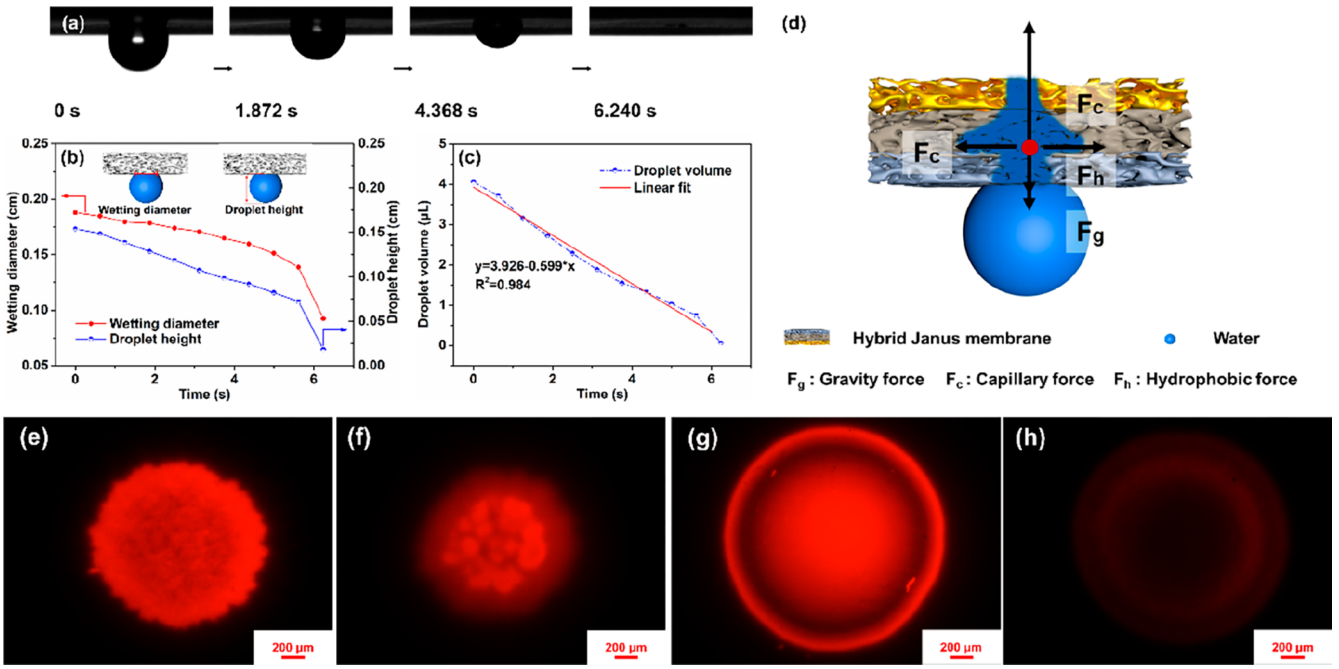

Figure 4. Self-pumping performance and micro-volume liquid permeation. (a) Picture of the self-pumping process of HJM from the hydrophobic side (~4 μL); (b) change of wetting diameter and droplet height during the self-pumping process; (c) change of droplet volume during the self-pumping process; (d) diagram of self-pumping force analysis. The main physical forces involved in the self-pumping process are the capillary force (F_c), hydrophobic force (F_h), and gravity force (F_g). (e,f) Penetration starts from the hydrophobic side, the wetting morphology of the hydrophobic surface and hydrophilic surface; (g,h) penetration starts from the hydrophilic side, the wetting morphology of the hydrophilic surface and hydrophobic surface. The tracer solution was dyed with pyronin G and the volume of the droplet was 1 μL.

directly revealed by EDX scan images in Figures 2d and S4 and Table S1. Gold (Au) element was uniformly distributed on the membrane surface with 22.82 at. % content, indicating the successful in situ generation of gold nanoparticles by electroless plating. Comparing the EDX results of the two sides of HJM, more intensive distribution of carbon (C) element with 74.36 at. % contents was derived from the insulate/hydrophobic side (Figure 2e), showing the reservation of organic substance. ATR−FTIR and XPS (Figure S5, Tables S1 and S2) characterized the chemical structure and surface composition of membranes before and after modification. The difference elements from ATR−FTIR and XPS results further verified the unique hybrid construction of HJM with asymmetric wettability and conductivity. LCSM has been used to verify the asymmetric hydrophobic and hydrophilic structure of HJM. The hydrophobic layer was stained with oil-soluble fluorescent dye (coumarin 6) by the roller-assisted surface hydrophobic modification. The hydrophilic surface remained dark (Figure 2f), while the hydrophobic surface of HJM was stained with fluorescent dye (Figure 2g), indicating the successful realization of one-side surface modification. For further evaluation of asymmetric wettability gradient, the cross-sectional image of HJM was also observed after the hydrophilic side was stained with rhodamine B (Figure 2h). The thickness of the hydrophobic layer was lesser than the hydrophilic layer. Overall, in situ electroless gold nanoparticle plating achieved asymmetric modification on HJM while retaining the asymmetric wettability.

3.2. Unidirectional and Self-Pumping Liquid Transport of the HJM Membranes. For ultra-low microfluidic sweat sensing, requirements like low sample volume, fast mass transport, and no backflow of soluble chemical reagents should be all met. Hence, a bioinspired structure with opposite wettability was introduced to the porous membrane to realize unique unidirectional liquid transport performance. By monitoring the status of the water droplet during the permeation process, dynamic WCA was used to verify the wettability of HJM surfaces. As displayed in Figure 3a, after the water droplet contacted with the hydrophobic side, WCA declined gradually, while the water droplet permeated through the membrane without surface diffusing. This result verified the existence of a hydrophobic coating layer and ensured the positive liquid transport (penetration from the hydrophobic side to the hydrophilic side) from the hydrophobic surface. On the hydrophilic side of HJM, the WCA decreased from 59 to 9° in 2.8 s, indicating the quick spread of the water droplet on the hydrophilic surface. Pure water flux has also been measured to characterize the unidirectional liquid transport performance of HJM, which was a critical factor in ultra-low-volume sweat sample analysis. As shown in Figure 3b, the pure water flux from the hydrophobic side generally increased with the applied pressure. When the permeation process started from the hydrophilic side, no obvious water could be detected until the applied pressure reached 2000 Pa. The minimum applied pressure needed for water to penetrate the membrane can be defined as breakthrough pressure ($P_{B.P}$). A tested breakthrough pressure of about 1737.66 Pa was needed for water to penetrate the membrane in the negative direction (penetration from the hydrophilic side to the hydrophobic side).

Simplified physical force analysis was considered for a better understanding of this unidirectional liquid transport of HJM, as presented in Figure 3c,d. Imbalanced forces composed of hydrostatic pressure (F_P), hydrophobic force (F_h), and capillary force (F_c) remained in the interface with opposite wettability. For the hydrophilic side, with the hydrostatic pressure and capillary force, water reached the interface

https://doi.org/10.1021/acsami.1c16820
ACS Appl. Mater. Interfaces 2022, 14, 9644−9654

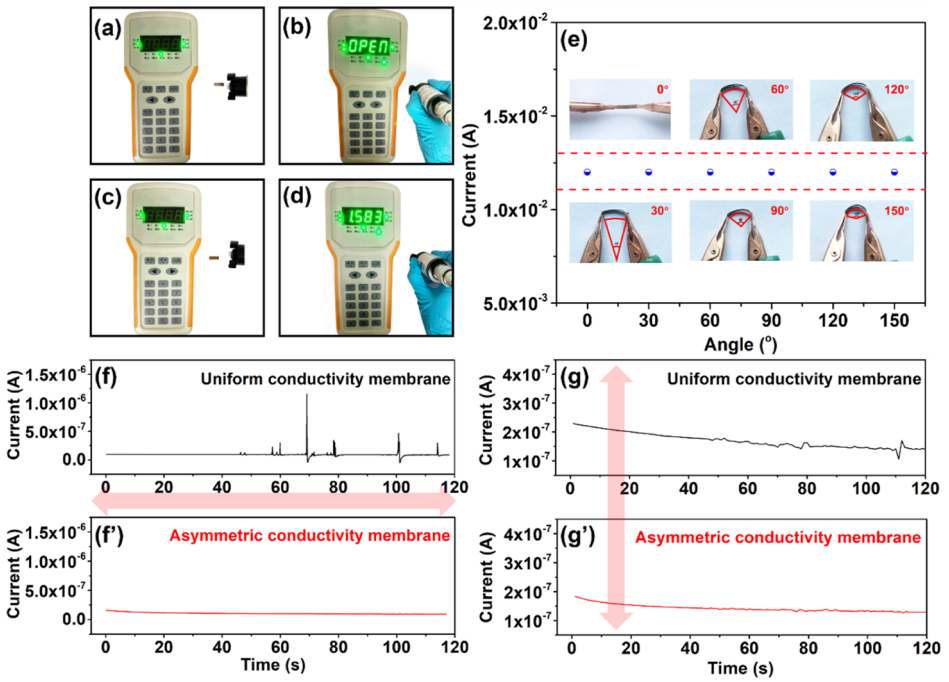

Figure 5. Asymmetric conductivity and anti-interference performance. (a–d) Surface resistance of HJM tested by a four-probe tester. (e) Conductivity of HJM at different bending angles. Current stability of uniform conductivity and HJM when friction interference was applied in different directions. (f,f′) *x*-axis direction; (g,g′) *y*-axis direction.

between the hydrophilic and hydrophobic layers. Subsequently, the penetration was blocked by the hydrophobic force, until the applied pressure was high enough ($P_{B.P}$) to overcome the resistance. The value of breakthrough pressure is mainly related to the capillary forces, which can be calculated by the Young–Laplace equation. After considering the influence of pore size and surface chemistry of the membrane, the equation can be rewritten as eqs 6 and 7.[39,44]

$$P_{B.P} = -P_{C.P} = -\frac{2\gamma}{r}\cos\theta = \frac{2\gamma(1-\cos\theta)}{R(\mu-1)(\mu-1+2\sin\theta)} \quad (6)$$

$$\mu = \frac{R+D}{R} = \frac{1}{\varphi} \quad (7)$$

where γ, r, θ, R, and μ are the liquid surface tension, membrane pore radius, contact angle between the liquid and the surface, cylinder radius, and dimensionless parameter, respectively. Apart from that, μ can be replaced by the reciprocal of membrane surface porosity (φ), as in eq 7. D represents the half spacing between the adjacent cylinder.

In this study, the water surface tension was 72.8 dyn/cm, membrane pore radius was 0.95 μm, WCA on pure hydrophobic coating was 125°, and the rough surface porosity of hydrophobic side was 8.36% taken from SEM images. The theoretical breakthrough pressure can be calculated as 1744.94 Pa, which is similar to the experimental value of 1737.66 Pa.

Sweat capture is the first step for precise detection of biomarkers in wearable electrochemical sweat biosensors. Apart from the unidirectional liquid transport performance, the efficiency of sample collection and micro-volume liquid transport is also of vital significance for detection at ultra-low volume in real time. Active liquid self-pumping performance of membranes for sweat collection was tested. As presented in Figure 4a, when the water droplet contacted the hydrophobic side of HJM, the droplet generally penetrated through the porous membrane. The volume of droplet decreased linearly at a fixed speed of 35.94 μL/min (Figure 4c). According to the evolution of wetting diameter and droplet height (Figure 4b), no surface diffusion was observed during the dynamic self-pumping process, showing a great potential for efficient sample collection. All the results indicated that the self-pumping process was driven by a stable and continuous force. The main physical forces involved in the self-pumping process are the capillary force (F_c), hydrophobic force (F_h), and gravity force (F_g). Among them, capillary force (F_c) and gravity force (F_g) play an opposite role in active liquid sucking, described in eqs 8 and 9, respectively.

$$F_c = 2\pi r\gamma\cos\theta \quad (8)$$

$$F_g = 2\pi r^2\rho g h \quad (9)$$

where γ, r, θ, ρ, g, and h are the liquid surface tension, membrane pore radius, contact angle between the liquid and the surface, liquid density, gravitational acceleration, and droplet height, respectively. The calculated capillary force was far larger than the gravity of the droplet itself, realizing the possibility of active self-pumping. Apart from theoretical calculation, LCSM images showed that water permeation could be achieved at a volume as low as 1 μL from the hydrophobic side without liquid backflow (Figure 4e–h). Micro-volume liquid focusing effect was further detected and the liquid absorption process was recorded (Figure S6). This effective transport of liquid is desired for sweat metabolite detection.

3.3. Asymmetric Conductivity and Anti-Interference Performance of the HJM Membranes. The stability of electric signal output is a key requirement for wearable sweat electrochemical sensors. Therefore, both flexibility and

https://doi.org/10.1021/acsami.1c16820
ACS Appl. Mater. Interfaces 2022, 14, 9644–9654

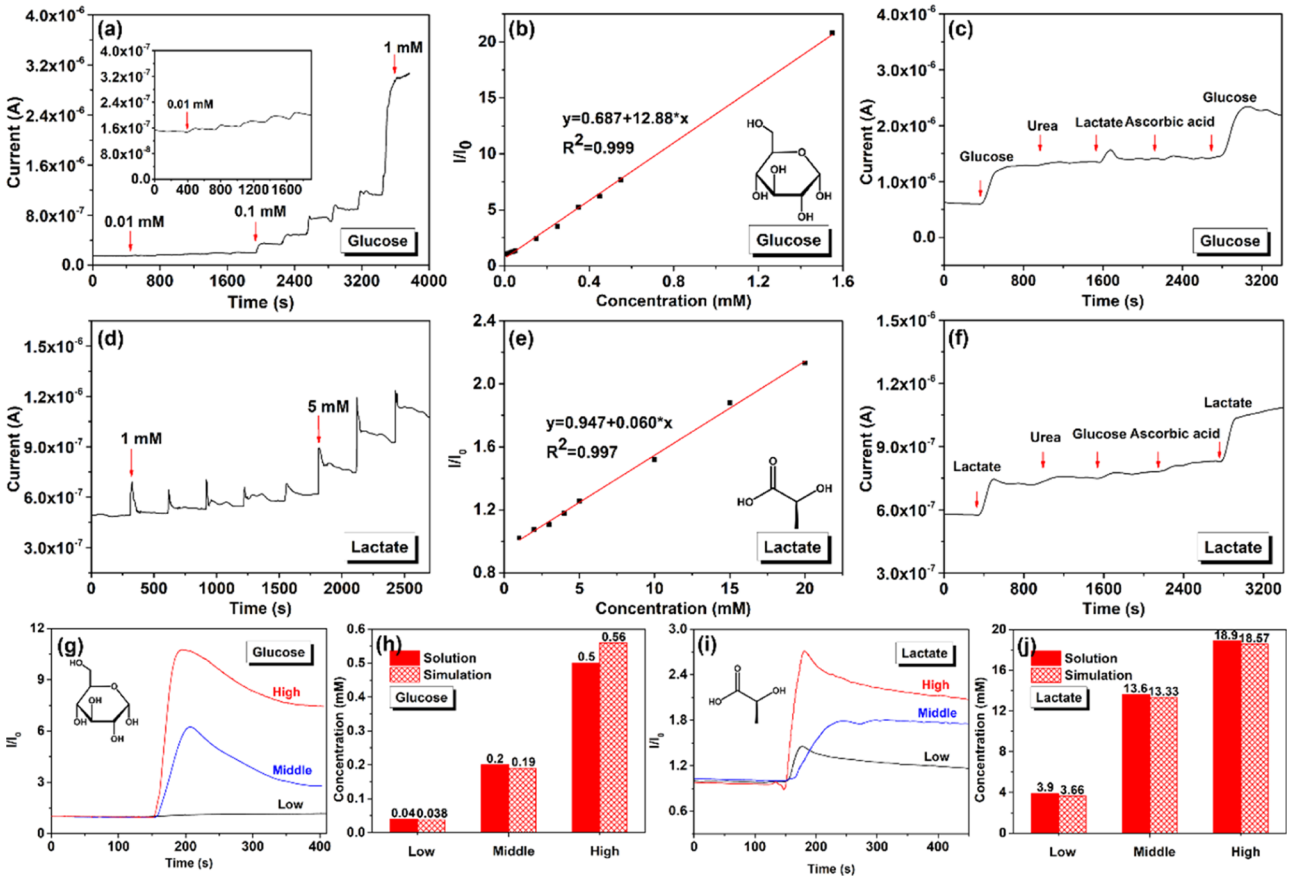

Figure 6. Electrochemical performance. (a,b,d,e) Chronoamperometric responses and sensitivity of glucose and lactate electrode to the respective analyte solutions in PBS. (c,f) Chronoamperometric response of the interference test for the glucose and lactate electrodes in PBS at a potential of 0.5 V with the addition of 0.1 mM glucose/5 mM lactate, 0.03 mM urea, 5 mM lactate/0.1 mM glucose, 0.01 mM ascorbic acid, and 0.1 mM glucose/5 mM lactate. (g,i) Simulation detection of glucose and lactate on the skin surface. (h,j) Comparison of the glucose and lactate concentrations between the solution and simulation, based on the corresponding chronoamperometric response.

conductivity are required for sweat monitoring on the three-dimensional curved sensing surface. The electrical resistance of hydrophobic and hydrophilic surfaces of HJM were measured by a four-point probe tester.[45] The resistance of the hydrophobic surface shown in Figure 5b was out of the measurement range, showing as open circuit, whereas the resistance of the hydrophilic surface was only 1.583 Ω (Figure 5d) equivalent to a resistivity of 5.54×10^{-6} Ω·cm. The different conductivities of the HJM surfaces proved the successful formation of continuous conductive layers on the hydrophilic side by floating electroless plating. The currents of HJM during the different bending processes were recorded. Constant current is observed in Figure 5e, with the results of steady LED lighting (Figure S7), indicating the great flexibility and stable conductivity of HJM.

The accuracy of detection in sweat biosensors can also be influenced by the signal interference of physical friction between the sensing element and the epidermis. An effective solution is to avoid the direct contact between the conductive materials and the epidermis, which is the original design intent of HJM with asymmetric conductivity. In Figure 5f–g′, the continuous current is recorded and compared between uniform conductivity membrane and HJM under friction in both *x*- and y-axes directions. The current curve of HJM was relatively smooth without obvious abrupt change in current, showing a promising anti-interference performance in wearable applications.

3.4. Electrochemical Performance of the Pt-Enzyme-HJM Electrodes. For the fabrication of the electrochemical electrode, single-side electro-deposition of Pt nanoparticles was applied to form the catalysis layer, which was significant for improving sensitivity and selectivity of detection.[46] The morphology of HJM after electro-deposition was observed by SEM (Figure S8). Nanoflower cluster was decorated on the Au layer, and the composition was detected by EDX (Figure S9, Table S4), indicating the successful deposition of the Pt catalytic layer. The analysis of elements on the membrane surface was taken by XPS (Figure S10, Table S5), further confirming the existence of the catalysis layer. In order to further verify the effectiveness of Pt deposition and catalysis activity, CVs of the bare HJM and Pt-decorated HJM electrode were recorded in a mixture solution of 5 mM $Fe(CN)_6^{3-/4-}$ and 0.1 M NaCl. Compared with the bare electrode, increased electron transfer rate (ΔE_p) and catalytic current were presented (Figure S11) in the modified electrode, due to the larger catalytic area of the Pt nanoflower cluster after electro-deposition.

In order to test the electrochemical monitoring performance of this HJM-based wearable biosensor, glucose and lactate were chosen as two typical targets of physiological metabolites in sweat. After specific enzyme immobilization, the Pt-enzyme-HJM electrodes were successfully prepared. The electrochemistry performance of Pt-enzyme-HJM electrodes was first measured in PBS solution with successive addition of

https://doi.org/10.1021/acsami.1c16820
ACS Appl. Mater. Interfaces 2022, 14, 9644−9654

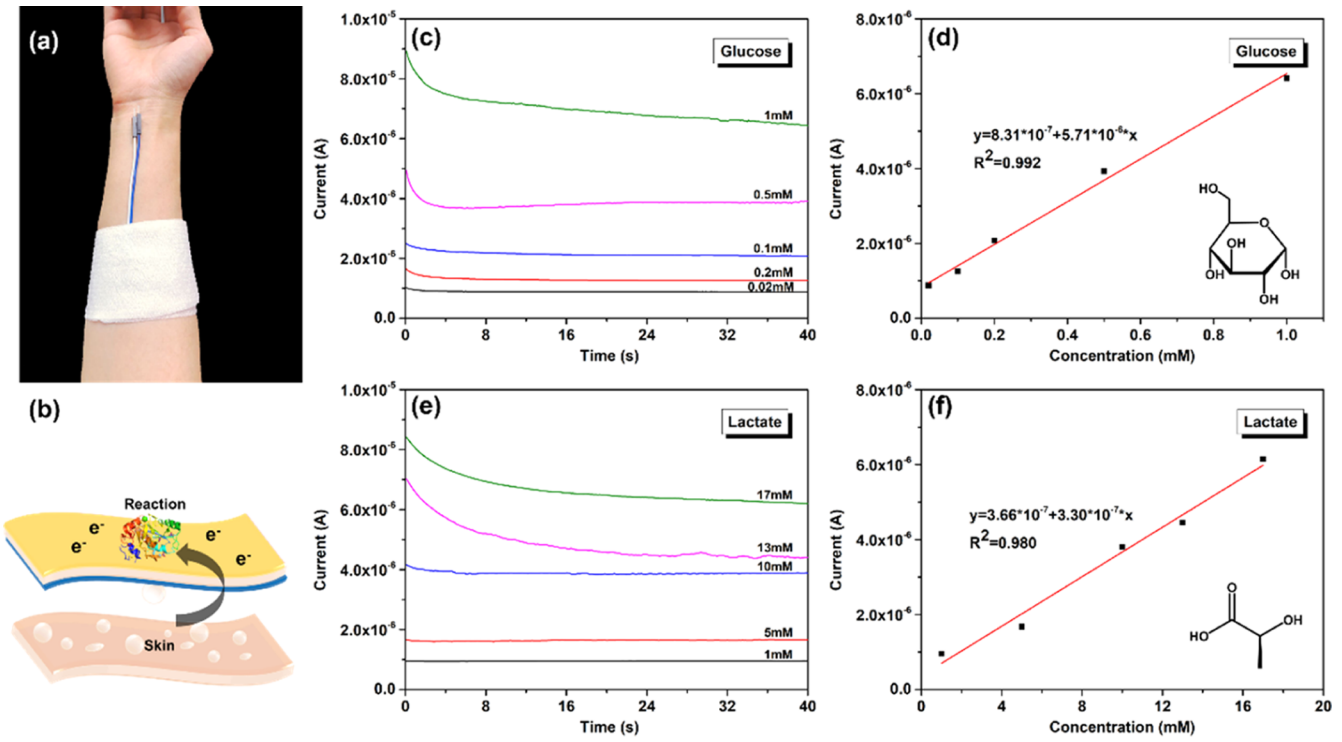

Figure 7. In situ monitoring of glucose and lactate on the skin surface. (a) Wearable biosensor attachment to the epidermis; (b) detection mechanism based on directional and self-pumping; (c,e) amperometric response curves of glucose and lactate; (d,f) sensitivity of glucose and lactate.

target analytes. With increasing concentration of analytes,[47] the currents of electrodes increased generally and reached a steady value. The membrane-based electrode after platinized showed low catalysis performance of the glucose among the test range (Figure S12). Oxidization by GOx enzyme played the main role in detection. A linear relationship was calculated over the glucose concentration range from 0.01−1.55 mM glucose concentration with a 0.999 correlation coefficient and 1.89 μA·mM^{-1} sensitivity (Figure 6a,b). In the detection of lactate (Figure 6d,e), the Pt-enzyme-HJM presented a linearity sensing between 0 and 20 mM (R^2 = 0.997) and a sensitivity of 29.2 nA·mM^{-1}. Both the detection ranges were designed according to the normal physiological condition in sweat. Compared with other works (Tables S6 and S7), desirable sensitivity for both glucose and lactate could be achieved, mainly due to high catalytic activity area of in situ Au/Pt nanoparticle generation on HJM. Also, the Pt-enzyme-HJM electrodes presented desirable operation stability when the test was repeated 6 times (Figure S13).

Because of the various electroactive species in sweat, sensing selectivity is also significant for accurate electrochemical detection. Urea, glucose, ascorbic acid, and lactate were injected into the solution as the interferents (Figure 6c,f).[48] The Pt-enzyme-HJM showed a current response to the addition of corresponding target analysts, while no obvious current change was recorded with the addition of interferences, indicating the specific recognition of electrodes.

For further ensuring the self-pumping, selectivity, and sensitivity performance of the Pt-enzyme-HJM electrodes, wearable sweat metabolite detection was performed on a simulated skin surface with an artificial perspiration process. In this experiment, a piece of wetting filter paper containing simulated sweat was used as the simulated skin surface. Eventually, specific molecular recognition was realized on the hydrophilic Pt-enzyme catalysis layer. Three different concentrations of glucose and lactate (low, middle, and high) were chosen, according to the corresponding level in the physiological range of sweat. The response current toward glucose and lactate is recorded in Figure 6g,i, used for the relevant calculation of concentrations from as-mentioned calibration curves. Apart from the current change, comparisons between the solutions and simulation experiments were done to demonstrate the accuracy of biosensors. As shown in Figure 6h, the deviated values of tested glucose concentration were 5, 5, and 12%, indicating desired accuracy of electrodes. In the detection of lactate (Figure 6j), 6.2, 2, and 1.7% bias were observed in low, middle, and high concentrations, respectively. Hence, the Pt-enzyme-HJM electrodes showed great potential in wearable sweat electrochemistry monitoring.

3.5. In Situ Sweat Metabolite Detection. The feasibility of the practical application of hybrid biosensors was performed by in situ detection of glucose and lactate. A miniaturized electrochemical workstation circuit was used to meet the needs of detection (Figure S14). The I−t curves were obtained from artificial sweat, while the biosensors were directly attached to the skin (Figure 7a). Specially, certain artificial sweat was pre-wetted on the epidermis for filling the sensing areas of biosensors (a low detection volume of ∼ 0.15 μL). The critical volume threshold (0.15 μL) for the available electrochemical detection was verified by a volume-dependent chronoamperometric experiment (Figure S15). The micro-volume sweat droplet was then up-taken into the porous electrode, where the glucose was electrochemically oxidized on the Pt-enzyme catalysis layer, leading to current changes, as presented in Figure 7b. Figure 7c shows the amperometric curves of sweat with different glucose levels in the range of 0.01−1 mM. The

https://doi.org/10.1021/acsami.1c16820
ACS Appl. Mater. Interfaces 2022, 14, 9644−9654

relationship between the recorded current and concentration (Figure 7d) matched with a linear regression equation (R^2 = 0.992), indicating high sensitivity, anti-interference, and micro-volume self-pumping performance of the biosensors. Besides, a similar current response was observed in lactate detection in the concentration range of 0−20 mM (Figure 7e). From Figure 7f, the linear relationship of lactate was derived with a correlation efficiency of 0.980. The Pt-enzyme-HJM could also be used for metabolite detection in real sweat with a shorter response time and sufficient monitoring accuracy (Figure S16). All in all, the hybrid biosensor integrated excellent liquid collection and metabolite detection function with desirable sensitivity, selectivity, and anti-interference, displaying great applicability in wearable sweat electrochemistry detection at ultra-low volume in real time.

4. CONCLUSIONS

A Janus membrane-based wearable biosensor with dual-asymmetry integration of wettability and conductivity was prepared by successive dip coating (PDA), roller-assisted liquid printing (fluoropolymer), and floating electroless gold plating. The breakthrough pressure of HJM was 1737.66 Pa, and the rate of water self-pumping was 35.94 μL/min. Due to the asymmetric wettability of HJM, unidirectional and self-pumping liquid transport performance were achieved simultaneously, preventing soluble chemical reagent backflow and effective sample collection in wearable sweat monitoring. The asymmetric conductive layer was generated from in situ generation of gold nanoparticles by platinum colloid-catalyzed gold electroless plating, showing superior flexible conductivity, excellent anti-interference of friction, and efficient electrochemical interface. Furthermore, Pt-enzyme-HJM electrodes showed great electrochemical performance in the detection of glucose and lactate with effective testing range, great selectivity, and high sensitivity and accuracy (correlation efficiency, glucose: R^2 = 0.999, lactate: R^2 = 0.997) in electrochemical detection. Moreover, the real time detection on the skin surface at ultra-low volume (~0.15 μL) was also realized. In summary, HJM with dual-asymmetry integration of wettability and conductivity shows great potential in the miniaturization of wearable sweat electrochemical biosensors for real-time measurement and multiplex analysis in athletic performance evaluation, health monitoring, disease diagnosis, intelligent medicine, and so forth.

■ ASSOCIATED CONTENT

Supporting Information

The Supporting Information is available free of charge at https://pubs.acs.org/doi/10.1021/acsami.1c16820.

Asymmetric wettability and enhanced interface floating performance of BJM membrane; optimization of enzyme content; surface and cross-sectional morphologies of the blank and BJM membranes; additional element distribution and compositions on the surface of HJM by EDX; ATR−FITR and XPS spectra of the blank, hydrophobic, and hydrophilic surfaces of BJM and HJM; surface compositions of the blank, both sides of BJM and HJM according to XPS spectra; micro-volume liquid focusing effect and liquid absorption of HJM membrane; great conductivity of HJM membrane; surface and cross-sectional morphologies of the HJM after Pt nanoparticle electrodeposition; element distribution and composition on the surface of HJM after Pt nanoparticle electrodeposition; XPS spectra and corresponding surface compositions (in atomic percentage) of HJM after Pt nanoparticle electrodeposition; CVs of the bare and platinized electrode; electrocatalysis performance of the HJM-based electrode after Pt nanoparticle electrodeposition; comparison of several wearable sweat sensors for glucose and lactate analysis; operation stability of Pt-enzyme-HJM electrodes; picture of a miniaturized electrochemical workstation circuit; volume-dependent chronoamperometric response; and real-time analysis results for in situ monitoring (PDF)

■ AUTHOR INFORMATION

Corresponding Authors

Dajing Chen − *School of Pharmacy, Hangzhou Normal University, Hangzhou 311121, China*; Email: djchen@hznu.edu.cn

Xiaojun Huang − *Key Laboratory of Macromolecular Synthesis and Functionalization, MOE Engineering Research Center of Membrane and Water Treatment Technology, Department of Polymer Science and Engineering, Zhejiang University, Hangzhou 310027, China*; orcid.org/0000-0003-4682-7364; Email: hxjzxh@zju.edu.cn

Authors

Xiao Hong − *Key Laboratory of Macromolecular Synthesis and Functionalization, MOE Engineering Research Center of Membrane and Water Treatment Technology, Department of Polymer Science and Engineering, Zhejiang University, Hangzhou 310027, China*

Huimin Wu − *Key Laboratory of Macromolecular Synthesis and Functionalization, MOE Engineering Research Center of Membrane and Water Treatment Technology, Department of Polymer Science and Engineering, Zhejiang University, Hangzhou 310027, China*

Chengcheng Wang − *School of Pharmacy, Hangzhou Normal University, Hangzhou 311121, China*

Xinran Zhang − *School of Pharmacy, Hangzhou Normal University, Hangzhou 311121, China*

Chenjie Wei − *Key Laboratory of Macromolecular Synthesis and Functionalization, MOE Engineering Research Center of Membrane and Water Treatment Technology, Department of Polymer Science and Engineering, Zhejiang University, Hangzhou 310027, China*

Zhikang Xu − *Key Laboratory of Macromolecular Synthesis and Functionalization, MOE Engineering Research Center of Membrane and Water Treatment Technology, Department of Polymer Science and Engineering, Zhejiang University, Hangzhou 310027, China*; orcid.org/0000-0002-2261-7162

Complete contact information is available at: https://pubs.acs.org/10.1021/acsami.1c16820

Notes

The authors declare no competing financial interest.

■ ACKNOWLEDGMENTS

The work was financially funded by National Natural Science Foundation of China (grant nos. 22075242 and 61801160) and the Basic Public Welfare Research Program of Zhejiang Province (no. LGG20E030005).

REFERENCES

(1) Li, S.; Ma, Z.; Cao, Z.; Pan, L.; Shi, Y. Advanced Wearable Microfluidic Sensors for Healthcare Monitoring. *Small* **2020**, *16*, No. e1903822.

(2) Su, Y.; Wang, J.; Wang, B.; Yang, T.; Yang, B.; Xie, G.; Zhou, Y.; Zhang, S.; Tai, H.; Cai, Z.; Chen, G.; Jiang, Y.; Chen, L.-Q.; Chen, J. Alveolus-inspired Active Membrane Sensors for Self-powered Wearable Chemical Sensing and Breath Analysis. *ACS Nano* **2020**, *14*, 6067−6075.

(3) Zhang, D.; Tang, Y.; Zhang, Y.; Yang, F.; Liu, Y.; Wang, X.; Yang, J.; Gong, X.; Zheng, J. Highly Stretchable, Self-adhesive, Biocompatible, Conductive Hydrogels as Fully Polymeric Strain Sensors. *J. Mater. Chem. A* **2020**, *8*, 20474−20485.

(4) He, J.; Xiao, P.; Lu, W.; Shi, J.; Zhang, L.; Liang, Y.; Pan, C.; Kuo, S.-W.; Chen, T. A Universal High Accuracy Wearable Pulse Monitoring System via High Sensitivity and Large Linearity Graphene Pressure Sensor. *Nano Energy* **2019**, *59*, 422−433.

(5) Wang, H.; Wang, H.; Wang, Y.; Su, X.; Wang, C.; Zhang, M.; Jian, M.; Xia, K.; Liang, X.; Lu, H.; Li, S.; Zhang, Y. Laser Writing of Janus Graphene/Kevlar Textile for Intelligent Protective Clothing. *ACS Nano* **2020**, *14*, 3219−3226.

(6) Pal, A.; Nadiger, V. G.; Goswami, D.; Martinez, R. V. Conformal, waterproof electronic decals for wireless monitoring of sweat and vaginal pH at the point-of-care. *Biosens. Bioelectron.* **2020**, *160*, 112206.

(7) Chen, M.-M.; Cheng, S.-B.; Ji, K.; Gao, J.; Liu, Y.-L.; Wen, W.; Zhang, X.; Wang, S.; Huang, W.-H. Construction of a flexible electrochemiluminescence platform for sweat detection. *Chem. Sci.* **2019**, *10*, 6295−6303.

(8) Wang, Z.; Hao, Z.; Wang, X.; Huang, C.; Lin, Q.; Zhao, X.; Pan, Y. A Flexible and Regenerative Aptameric Graphene-nafion Biosensor for Cytokine Storm Biomarker Monitoring in Undiluted Biofluids Toward Wearable Applications. *Adv. Funct. Mater.* **2020**, *31*, 2005958.

(9) Yang, Y.; Gao, W. Wearable and Flexible Electronics for Continuous Molecular Monitoring. *Chem. Soc. Rev.* **2019**, *48*, 1465−1491.

(10) Wang, Y.; Zhao, C.; Wang, J.; Luo, X.; Xie, L.; Zhan, S.; Kim, J.; Wang, X.; Liu, X.; Ying, Y. Wearable Plasmonic-metasurface Sensor for Noninvasive and Universal Molecular Fingerprint Detection on Biointerfaces. *Sci. Adv.* **2021**, *7*, No. eabe4553.

(11) Zhao, Z.; Kong, Y.; Lin, X.; Liu, C.; Liu, J.; He, Y.; Yang, L.; Huang, G.; Mei, Y. Oxide nanomembrane induced assembly of a functional smart fiber composite with nanoporosity for an ultra-sensitive flexible glucose sensor. *J. Mater. Chem. A* **2020**, *8*, 26119−26129.

(12) Brothers, M. C.; DeBrosse, M.; Grigsby, C. C.; Naik, R. R.; Hussain, S. M.; Heikenfeld, J.; Kim, S. S. Achievements and Challenges for Real-time Sensing of Analytes in Sweat Within Wearable Platforms. *Acc. Chem. Res.* **2019**, *52*, 297−306.

(13) Promphet, N.; Hinestroza, J. P.; Rattanawaleedirojn, P.; Soatthiyanon, N.; Siralertmukul, K.; Potiyaraj, P.; Rodthongkum, N. Cotton Thread-based Wearable Sensor for Non-invasive Simultaneous Diagnosis of Diabetes and Kidney Failure. *Sens. Actuators, B* **2020**, *321*, 128549.

(14) Liu, X.; Zhang, W.; Lin, Z.; Meng, Z.; Shi, C.; Xu, Z.; Yang, L.; Liu, X. Y. Coupling of Silk Fibroin Nanofibrils Enzymatic Membrane with Ultra-Thin PtNPs/Graphene Film to Acquire Long and Stable On-Skin Sweat Glucose and Lactate Sensing. *Small Methods* **2021**, *5*, 2000926.

(15) Zhai, Q.; Gong, S.; Wang, Y.; Lyu, Q.; Liu, Y.; Ling, Y.; Wang, J.; Simon, G. P.; Cheng, W. Enokitake Mushroom-like Standing Gold Nanowires Toward Wearable Noninvasive Bimodal Glucose and Strain Sensing. *ACS Appl. Mater. Interfaces* **2019**, *11*, 9724−9729.

(16) Wiorek, A.; Parrilla, M.; Cuartero, M.; Crespo, G. A. Epidermal Patch with Glucose Biosensor: pH and Temperature Correction Toward More Accurate Sweat Analysis during Sport Practice. *Anal. Chem.* **2020**, *92*, 10153−10161.

(17) Toi, P. T.; Trung, T. Q.; Dang, T. M. L.; Bae, C. W.; Lee, N.-E. Highly Electrocatalytic, Durable, and Stretchable Nanohybrid Fiber for On-body Sweat Glucose Detection. *ACS Appl. Mater. Interfaces* **2019**, *11*, 10707−10717.

(18) Liu, Q.; Liu, Y.; Wu, F.; Cao, X.; Li, Z.; Alharbi, M.; Abbas, A. N.; Amer, M. R.; Zhou, C. Highly Sensitive and Wearable In_2O_3 Nanoribbon Transistor Biosensors with Integrated On-chip Gate for Glucose Monitoring in Body Fluids. *ACS Nano* **2018**, *12*, 1170−1178.

(19) Koh, A.; Kang, D.; Xue, Y.; Lee, S.; Pielak, R. M.; Kim, J.; Hwang, T.; Min, S.; Banks, A.; Bastien, P.; Manco, M. C.; Wang, L.; Ammann, K. R.; Jang, K.; Won, P.; Han, S.; Ghaffari, R.; Paik, U.; Slepian, M. J.; Balooch, G.; Huang, Y.; Rogers, J. A. A soft, wearable microfluidic device for the capture, storage, and colorimetric sensing of sweat. *Sci. Transl. Med.* **2016**, *8*, 366ra165.

(20) Bae, C. W.; Toi, P. T.; Kim, B. Y.; Lee, W. I.; Lee, H. B.; Hanif, A.; Lee, E. H.; Lee, N.-E. Fully Stretchable Capillary Microfluidics-integrated Nanoporous Gold Electrochemical Sensor for Wearable Continuous Glucose Monitoring. *ACS Appl. Mater. Interfaces* **2019**, *11*, 14567−14575.

(21) He, W.; Wang, C.; Wang, H.; Jian, M.; Lu, W.; Liang, X.; Zhang, X.; Yang, F.; Zhang, Y. Integrated Textile Sensor Patch for Real-time and Multiplex Sweat Analysis. *Sci. Adv.* **2019**, *5*, No. eaax0649.

(22) Oh, S. Y.; Hong, S. Y.; Jeong, Y. R.; Yun, J.; Park, H.; Jin, S. W.; Lee, G.; Oh, J. H.; Lee, H.; Lee, S.-S.; Ha, J. S. Skin-attachable, Stretchable Electrochemical Sweat Sensor for Glucose and pH Detection. *ACS Appl. Mater. Interfaces* **2018**, *10*, 13729−13740.

(23) Koh, A.; Kang, D.; Xue, Y.; Lee, S.; Pielak, R. M.; Kim, J.; Hwang, T.; Min, S.; Banks, A.; Bastien, P.; Manco, M. C.; Wang, L.; Ammann, K. R.; Jang, K.; Won, P.; Han, S.; Ghaffari, R.; Paik, U.; Slepian, M. J.; Balooch, G.; Huang, Y.; Rogers, J. A. A Soft, Wearable Microfluidic Device for the Capture, Storage, and Colorimetric Sensing of Sweat. *Sci. Transl. Med.* **2016**, *8*, 366ra165.

(24) Jeong, W.; Song, J.; Bae, J.; Nandanapalli, K. R.; Lee, S. Breathable Nanomesh Humidity Sensor for Real-time Skin Humidity Monitoring. *ACS Appl. Mater. Interfaces* **2019**, *11*, 44758−44763.

(25) Peng, R.; Sonner, Z.; Hauke, A.; Wilder, E.; Kasting, J.; Gaillard, T.; Swaille, D.; Sherman, F.; Mao, X.; Hagen, J.; Murdock, R.; Heikenfeld, J. A new oil/membrane approach for integrated sweat sampling and sensing: sample volumes reduced from μL's to nL's and reduction of analyte contamination from skin. *Lab Chip* **2016**, *16*, 4415−4423.

(26) Cao, Q.; Liang, B.; Tu, T.; Wei, J.; Fang, L.; Ye, X. Three-dimensional Paper-based Microfluidic Electrochemical Integrated Devices (3D-PMED) for Wearable Electrochemical Glucose Detection. *RSC Adv.* **2019**, *9*, 5674−5681.

(27) Noviana, E.; McCord, C. P.; Clark, K. M.; Jang, I.; Henry, C. S. Electrochemical Paper-based Devices: Sensing Approaches and Progress Toward Practical Applications. *Lab Chip* **2020**, *20*, 9−34.

(28) Xu, Y.; Zhao, G.; Zhu, L.; Fei, Q.; Zhang, Z.; Chen, Z.; An, F.; Chen, Y.; Ling, Y.; Guo, P.; Ding, S.; Huang, G.; Chen, P.-Y.; Cao, Q.; Yan, Z. Pencil-paper On-skin Electronics. *Proc. Natl. Acad. Sci. U.S.A.* **2020**, *117*, 18292−18301.

(29) Yan, S.; Shan, S.; Wen, J.; Li, J.; Kang, N.; Wu, Z.; Lombardi, J.; Cheng, H. W.; Wang, J.; Luo, J.; He, N.; Mott, D.; Wang, L.; Ge, Q.; Hsiao, B. S.; Poliks, M.; Zhong, C. J. Surface-mediated Interconnections of Nanoparticles in Cellulosic Fibrous Materials toward 3D Sensors. *Adv. Mater.* **2020**, *32*, No. e2002171.

(30) Madhu, S.; Anthuuvan, A. J.; Ramasamy, S.; Manickam, P.; Bhansali, S.; Nagamony, P.; Chinnuswamy, V. ZnO Nanorod Integrated Flexible Carbon Fibers for Sweat Cortisol Detection. *ACS Appl. Mater. Interfaces* **2020**, *2*, 499−509.

(31) He, X.; Fan, C.; Xu, T.; Zhang, X. Biospired Janus Silk E-textiles with Wet-thermal Comfort for Highly Efficient Biofluid Monitoring. *Nano Lett.* **2021**, *21*, 8880−8887.

(32) Zhao, Y.; Zhai, Q.; Dong, D.; An, T.; Gong, S.; Shi, Q.; Cheng, W. Highly Stretchable and Strain-insensitive Fiber-based Wearable Electrochemical Biosensor to Monitor Glucose in the Sweat. *Anal. Chem.* **2019**, *91*, 6569−6576.

https://doi.org/10.1021/acsami.1c16820
ACS Appl. Mater. Interfaces 2022, 14, 9644−9654

(33) He, X.; Yang, S.; Pei, Q.; Song, Y.; Liu, C.; Xu, T.; Zhang, X. Integrated Smart Janus Textile Bands for Self-pumping Sweat Sampling and Analysis. *ACS Sens.* **2020**, *5*, 1548−1554.
(34) He, W.; Wang, C.; Wang, H.; Jian, M.; Lu, W.; Liang, X.; Zhang, X.; Yang, F.; Zhang, Y. Integrated Textile Sensor Patch for Real-time and Multiplex Sweat Analysis. *Sci. Adv.* **2019**, *5*, No. eaax0649.
(35) Emaminejad, S.; Gao, W.; Wu, E.; Davies, Z. A.; Yin Yin Nyein, H.; Challa, S.; Ryan, S. P.; Fahad, H. M.; Chen, K.; Shahpar, Z.; Talebi, S.; Milla, C.; Javey, A.; Davis, R. W. Autonomous Sweat Extraction and Analysis Applied to Cystic Fibrosis and Glucose Monitoring Using a Fully Integrated Wearable Platform. *Proc. Natl. Acad. Sci. U.S.A.* **2017**, *114*, 4625−4630.
(36) Lin, K.-C.; Muthukumar, S.; Prasad, S. Flex-GO (Flexible Graphene Oxide) Sensor for Electrochemical Monitoring Lactate in Low-volume Passive Perspired Human Sweat. *Talanta* **2020**, *214*, 120810.
(37) Twine, N. B.; Norton, R. M.; Brothers, M. C.; Hauke, A.; Gomez, E. F.; Heikenfeld, J. Open Nanofluidic Films with Rapid Transport and No Analyte Exchange for Ultra-low Sample Volumes. *Lab Chip* **2018**, *18*, 2816−2825.
(38) Xiao, J.; Liu, Y.; Su, L.; Zhao, D.; Zhao, L.; Zhang, X. Microfluidic Chip-Based Wearable Colorimetric Sensor for Simple and Facile Detection of Sweat Glucose. *Anal. Chem.* **2019**, *91*, 14803−14807.
(39) Hong, X.; Wu, H.-m.; Zhang, X.-r.; Wei, C.-j.; Chen, D.-j.; Huang, X.-j. The Micro-volume Liquid Focusing Effect in Janus Membrane and its Biosensing Application. *J. Colloid Interface Sci.* **2021**, *592*, 22−32.
(40) Horiuchi, S.; Nakao, Y. Platinum Colloid Catalyzed Etchingless Gold Electroless Plating with Strong Adhesion to Polymers. *Surf. Coat. Technol.* **2010**, *204*, 3811−3817.
(41) Al-Sagur, H.; Shanmuga Sundaram, K.; Kaya, E. N.; Durmuş, M.; Basova, T. V.; Hassan, A. Amperometric Glucose Biosensing Performance of a Novel Graphene Nanoplatelets-iron Phthalocyanine Incorporated Conducting Hydrogel. *Biosens. Bioelectron.* **2019**, *139*, 111323.
(42) Suman, S.; Singhal, R.; Sharma, A. L.; Malthotra, B. D.; Pundir, C. S. Development of a Lactate Biosensor Based on Conducting Copolymer Bound Lactate Oxidase. *Sens. Actuators, B* **2005**, *107*, 768−772.
(43) Ma, Z.; Luo, Y.; Zhu, Q.; Jiang, M.; Pan, M.; Xie, T.; Huang, X.; Chen, D. In-situ Monitoring of Glucose Metabolism in Cancer Cell Microenvironments Based on Hollow Fiber Structure. *Biosens. Bioelectron.* **2020**, *162*, 112261.
(44) Gupta, P.; Kandasubramanian, B. Directional Fluid Gating by Janus Membranes with Heterogeneous Wetting Properties for Selective Oil-water Separation. *ACS Appl. Mater. Interfaces* **2017**, *9*, 19102−19113.
(45) Zheng, X.; Li, L.; Cui, K.; Zhang, Y.; Zhang, L.; Ge, S.; Yu, J. Ultrasensitive Enzyme-free Biosensor by Coupling Cyclodextrin Functionalized Au Nanoparticles and High-performance Au-paper Electrode. *ACS Appl. Mater. Interfaces* **2018**, *10*, 3333−3340.
(46) Wu, H.; Zhang, X.; Wei, C.; Wang, C.; Jiang, M.; Hong, X.; Xu, Z.; Chen, D.; Huang, X. Modular Assembly of Enzyme Loaded Nanoparticles in 3D Hollow Fiber Electrode for Electrochemical Sensing. *Chem. Eng. J.* **2021**, *421*, 129721.
(47) Gao, W.; Emaminejad, S.; Nyein, H. Y. Y.; Challa, S.; Chen, K.; Peck, A.; Fahad, H. M.; Ota, H.; Shiraki, H.; Kiriya, D.; Lien, D.-H.; Brooks, G. A.; Davis, R. W.; Javey, A. Fully integrated wearable sensor arrays for multiplexed in situ perspiration analysis. *Nature* **2016**, *529*, 509−514.
(48) Wu, Q.; Hou, Y.; Zhang, M.; Hou, X.; Xu, L.; Wang, N.; Wang, J.; Huang, W. Amperometric Cholesterol Biosensor Based on Zinc Oxide Films on a Silver Nanowire-graphene Oxide Modified Electrode. *Anal. Methods* **2016**, *8*, 1806−1812.

https://doi.org/10.1021/acsami.1c16820
ACS Appl. Mater. Interfaces 2022, 14, 9644−9654